Supplementary Material for:" Achieving high-security and massive-capacity optical communications based on OAM configured chaotic laser "

Yanwei Cui[a], **Jianguo Zhang**[a,*], **Zhongquan Nie**[b*], **Anbang Wang**[c,d*], **Yuncai Wang**[c,d]
[a]Taiyuan University of Technology, Key Laboratory of Advanced Transducers and Intelligent Control System, Ministry of Education of China, College of Electronic Information and Optical Engineering, Taiyuan, China, 030024
[b]National University of Defense Technology, College of Advanced Interdisciplinary Studies, Changsha, China, 410073
[c]Guangdong University of Technology, School of Information Engineering, Guangzhou, China, 510006
[d]Guangdong Provincial Key Laboratory of Photonics Information Technology, Guangzhou, China, 510006

*Jianguo Zhang, zhangjianguo@tyut.edu.cn
*Zhongquan Nie, niezhongquan1018@163.com
*Anbang Wang, abwang@gdut.edu.cn

1 The basic principle of OAM-CCL

In this paper, we present a conceptual paradigm for orbital angular momentum (OAM) configured chaotic laser, as illustrated in Fig. S1. The experimental setup initiates with a semiconductor laser SL_D in a stable Gaussian mode. By introducing optical feedback, the laser undergoes a transition into a chaotic state, enhancing its dynamical complexity. After passing through the polarization controller and optical isolator, the chaotic laser is then coupled from the single-mode fiber into free space through the collimator. An important aspect of our approach is to manipulate the spatial patterns of a chaotic laser. This is achieved using a spatial light modulator (SLM) loaded with different holographic phase patterns, enabling the laser to carry different orbital angular momentum.

The fusion of OAM and chaotic laser expands the system's capabilities beyond traditional temporal considerations, allowing precise manipulation of the emitted light's spatial properties. Our novel chaotic laser technology blends chaos dynamics with OAM-carrying beams, offering versatility and extending utility to communication, sensing, and imaging domains.

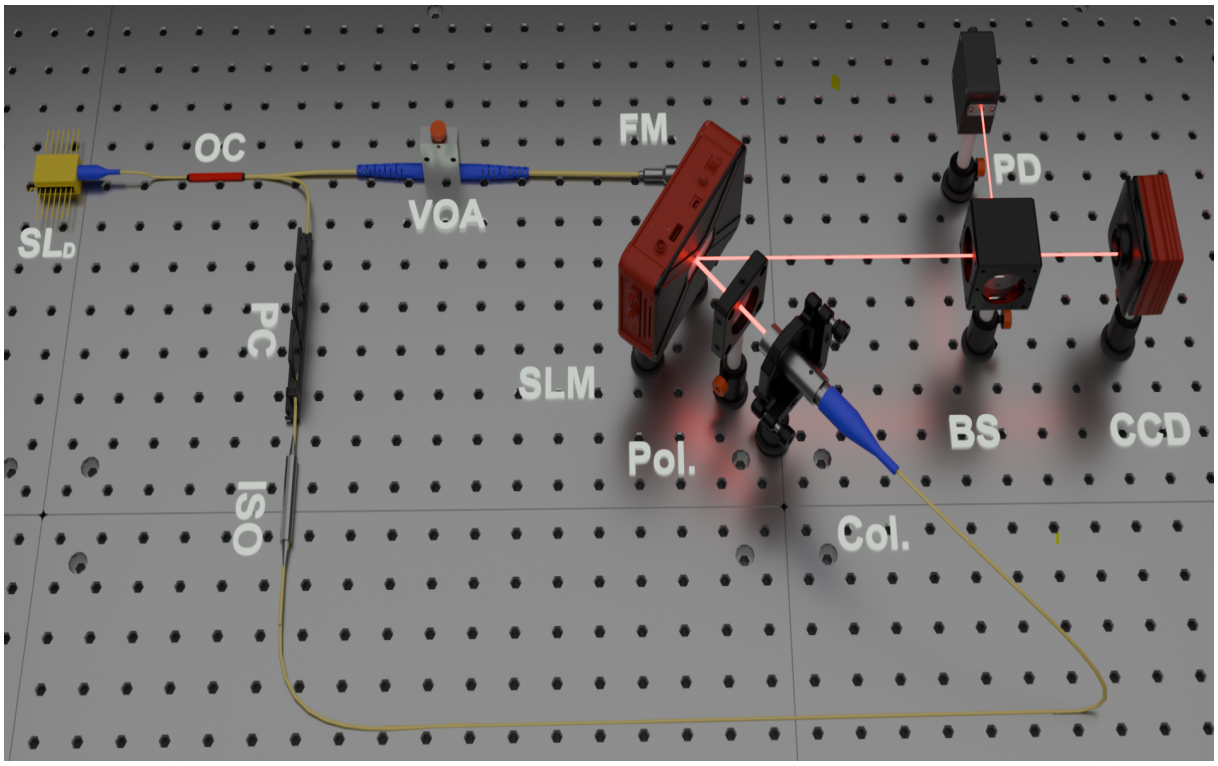

Fig S1 The schematic diagram of the OAM-CCL.

2 Multiplexing in OAM-CCL optical communication system

The encrypted signal transmitted in space can be expressed as:[17]

$$E_n^{enc}(r,t) = [E_n(t) + aE_{ch}(t)] \cdot A(r)\,. \tag{S1}$$

Where r is the radial distance from the optical axis, $E_0(t)$ and $E_{ch}(t)$ respectively represent the original signal and chaotic signal, $A(r) \propto exp(-r^2/\omega_0^2)$ is the complex electric field amplitude at the waist of the Gaussian beam. The signal converted by the spatial light modulator is expressed as:[17]

$$E_n^{enc}(r,\phi,t) = [E_n(t) + aE_{ch}(t)] \cdot A(r) \cdot exp(-il\phi)\,. \tag{S2}$$

Where the l is the angular quantum number, ϕ is the transverse azimuthal angle. For the multiplexed beam, which can be expressed as:

$$E_{mux}(r,\phi,t) = \sum_{p=0}^{N} E_p(t) \cdot A_p(r) \cdot exp(-il_p\phi)\,. \tag{S3}$$

Where $E_p(t)$ represents different signal loaded in different OAM modes. After demultiplexing the beam at the receiving end, the field can be expressed as:

$$E_{demux}(r,\phi,t)' = E_q(t)A_q(r)' + \sum_{p=0,p\neq q}^{N} E_p(t) \cdot A_p(r)' \cdot exp(-il_{p-q}\phi)\,. \tag{S4}$$

After filtering, the first term on the right-hand side of the equation is retained, while the other terms are removed, thus restoring the signal of the individual channels.

3 Chaos synchronization and chaos encryption

Equations S5, S6 and S7 describe the dynamics of chaos synchronization in the OAM-CCL optical communication system.

$$\begin{aligned}\frac{dE_D(r,\theta,t)}{dt} =& \frac{1}{2}(1+i\alpha)(G_D-\tau_p^{-1})E_D(t)exp(-\frac{r^2}{w_0^2})exp(-il\theta)+\\ & \kappa_f\tau_{in}^{-1}E_D(t-\tau_f)exp(-\frac{r_2}{w_0^2})exp(-il\theta)e^{-i\omega_0\tau_f}+F_D,\end{aligned} \tag{S5}$$

$$\begin{aligned}\frac{dE_{T,R}(r,\theta,t)}{dt} =& \frac{1}{2}(1+i\alpha)(G_{T,R}-\tau_p^{-1})E_{T,R}(t)exp(-\frac{r^2}{w_0^2})exp(-il\theta)+\\ & \kappa_j\tau_{in}^{-1}E_{T,R}(t-\tau_j)exp(-\frac{r^2}{w_0^2})exp(-il\theta)e^{-i(\omega_0\tau_j+\Delta\omega_{T,R}t)}+F_{T,R},\end{aligned} \tag{S6}$$

$$\frac{dN(t)}{dt} = (qV)^{-1} I_{D,T,R} - \tau_N^{-1} N_{D,T,R} - G_{D,T,R}|E_{D,T,R}|^2. \tag{S7}$$

Where $E(t)$ is the slowly varying complex amplitude of the electric field, and N is the carrier density. (r, θ) is the cylindrical coordinate, and w_0 is beam waist, $E(r, \theta, t)$ represent the space-time electric field of the chaotic laser. The subscripts D, T, R, stand for lasers $\mathrm{SL_D}$, $\mathrm{SL_T}$, $\mathrm{SL_R}$, respectively. τ_f and τ_j separately denote the feedback delay and injection delay, κ_f and κ_j separately denote the optical feedback strength and optical injection strength. $F_{D,T,R}$ denotes the Langevin noise caused by spontaneous radiation, which can be sescribe as $F_{D,T,R} = sqrt(2\beta N(t))\chi$, β is the spontaneous emission coefficient, χ is independent random variables. $G_{D,T,R}$ denotes optical gain, which can be sescribe as $G_{D,T,R} = g[N(t) - N_0]/[1 + \varepsilon E(t)^2]$. α, τ_p and τ_{in} separately denote linewidth enhancement factor, photon lifetime and round-trip time in laser cavity. q, V and τ_N separately denote elementary charge, active layer volume and carrier lifetime. $I_{D,T,R}$ denotes bias current.

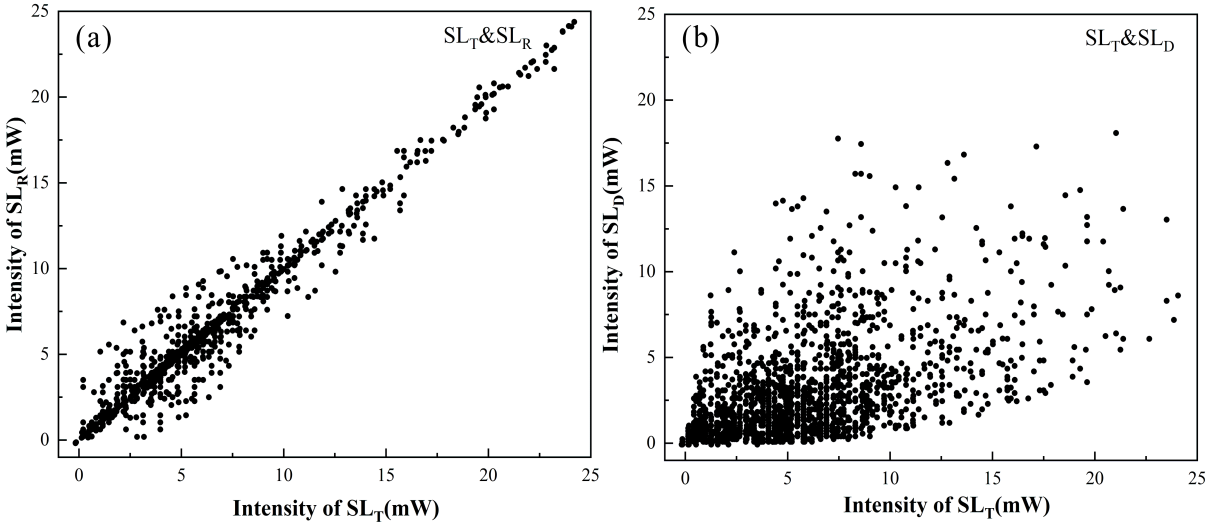

Fig S2 Correlation plots: (a) SLT and SLR; (b) SLD and SLT.

Unlike the classical Lang-Kobayashi equations, which only address the temporal aspects of

chaotic lasers, our equations incorporate spatially relevant parameters of the electric field to capture the unique spatio-temporal structure of OAM-CCL. Neglecting these spatial parameters reduces our equation to the classical Lang-Kobayashi equation.[37] When considering the entire equation, it reflects the varying temporal chaos alongside stable spatial orbital angular momentum in OAM-CCL.

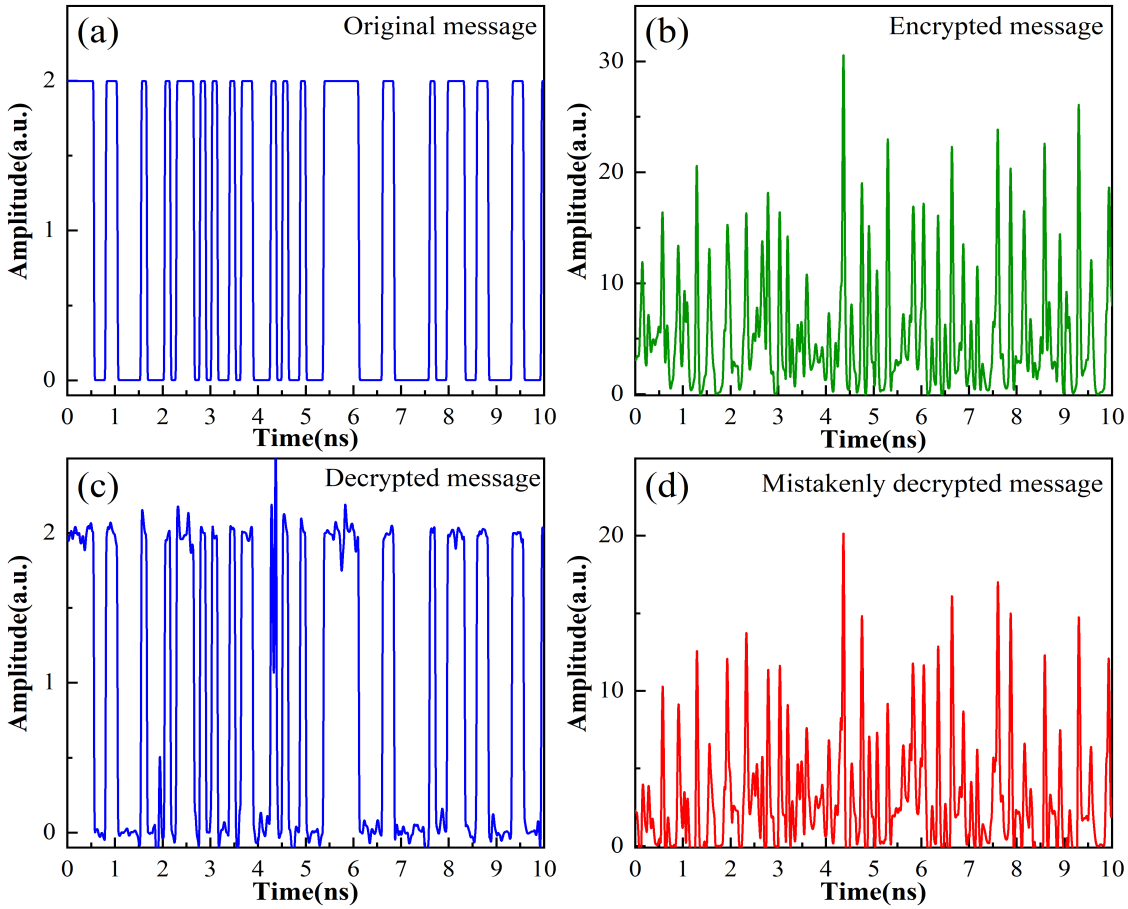

Fig S3 Message encryption and decryption: (a) original message; (b)encrypted message;(c) decrypted message; (d) Mistakenly decrypted message.

In our setup, the synchronization coefficient between the output of the semiconductor laser $\mathrm{SL_D}$ and the outputs of $\mathrm{SL_R}$ and $\mathrm{SL_T}$ is low, measuring 0.763, as demonstrated in Fig. S2. Conversely, the synchronization coefficient between the outputs of $\mathrm{SL_T}$ and $\mathrm{SL_R}$ is high, reaching 0.976. As a result, we can effectively employ the outputs of $\mathrm{SL_T}$ and $\mathrm{SL_R}$ for encryption and decryption of

information signals, respectively.

Figure S3 (a) shows the waveform of the original signal. Figure S3 (b) shows the waveform of the encrypted signal. Figure S3 (c) shows the waveform of the signal after correct decryption. Figure S3 (d) depicts the signal after an eavesdropper attempts to decrypt it using driving chaotic signal. The results show that because the correlation between driven chaotic signal and mask chaotic signal is very small, using driving chaotic signal to decrypt is ineffective for the eavesdropper.

4 Simulation parameters of chaotic laser

In order to achieve a more realistic simulation, our study utilized VPI TransmissionMaker software to simulate the chaotic semiconductor laser, with the main parameters presented in Table S1.

Table S1 Main simulation parameters and values for chaotic lasers

Symbol	Parameter	Value
N_0	Transparent carrier density/m^{-3}	1.0×10^{24}
σ	Linewidth enhancement factor	3.0
ϵ	Gain saturation parameters /m^3	1.0×10^{-23}
N_I	Carrier density /m^{-3}	1.5×10^{24}
T_g	Grating period /m	200×10^{-9}
G	Linear gain coefficient /m^2	3×10^{-20}
L	Length of active area /um	250
W	Width of active zone /um	2.5
B_n	Spontaneous radiated noise bandwidth /THz	10
B_g	Gain bandwidth/THz	20
n	Group refractivity	3.7
I_{th}	Threshold current/mA	20

5 eavesdropping resistance

In free-space optical communication links based on conventional Gaussian beams, eavesdroppers retain the ability to intercept a portion of the transmitted beam energy along the transmission path.[59] In contrast, the OAM-CCL communication system exhibits better eavesdropping resistance. Notably, the orbital angular momentum beam exhibits the angular uncertainty principle in macroscopic observations, whereby smaller observation apertures or inappropriate observation positions can result in significant power degradation and crosstalk within the OAM modes observed by the eavesdropper.[58]

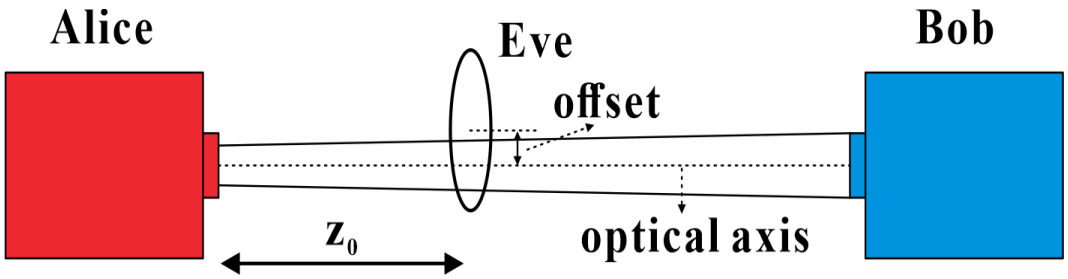

Fig S4 Schematic diagram of eavesdropping channel based on OAM-CCL communication system.

To demonstrate the eavesdropping resistance of OAM-CCL system, we build an eavesdropping channel as shown in Fig. S4. In this setup, we assume that the beam waist of the emitted beam is 5 mm, and Eve is positioned at a distance of 100 m from Alice. When the deviation of the center of Eve from the optical axis is 2 mm, the crosstalk matrix of each channel tapped by Eve is shown in Fig. S5.

To quantify the eavesdropping ability of Eve, we define the eavesdropping coefficient:

$$\gamma_{Eve} = 10 \log \left(P_s / P_n \right), \tag{S8}$$

where P_s denotes the mode power that Eve receives correctly, and P_n denotes the mode power that

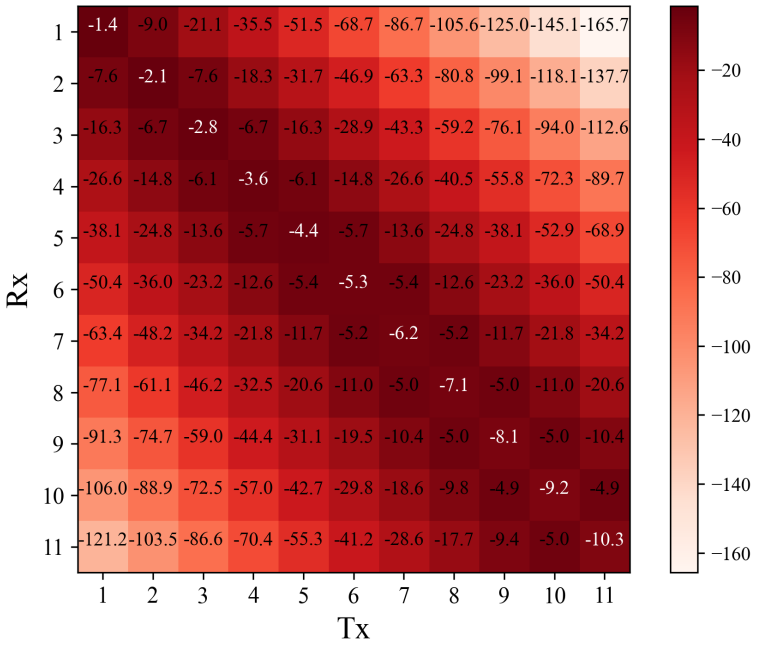

Fig S5 Crosstalk matrix for each channel tapped by Eve.

Eve fails to receive correctly, which will leak to other modes causing crosstalk.

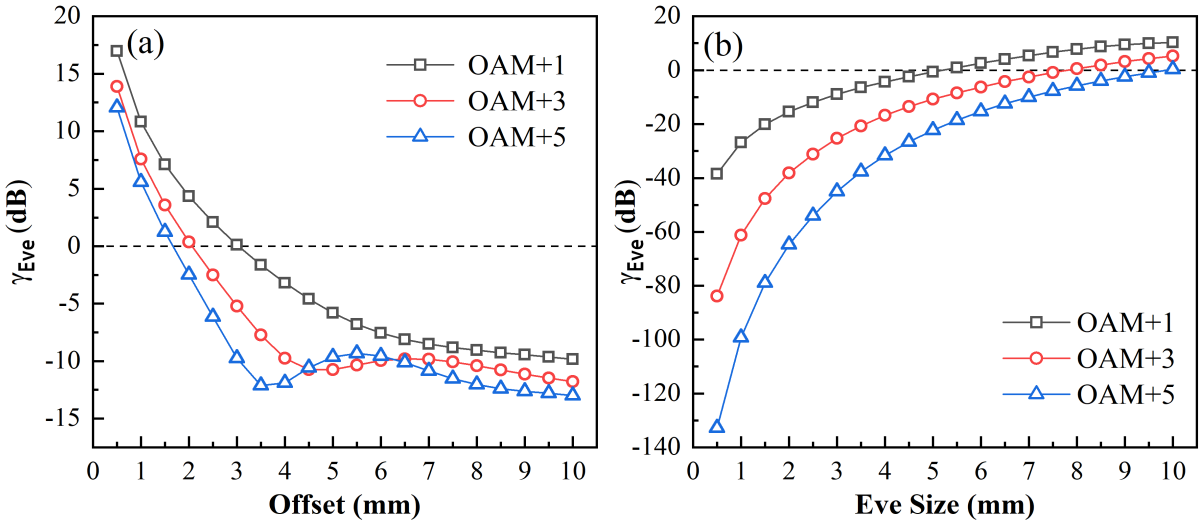

Fig S6 Eve's eavesdropping coefficient (a) Offset versus eavesdropping coefficient; (b) Eve size versus eavesdropping coefficient.

Figure S6(a) illustrates the relationship between the offset and the eavesdropping coefficient when Eve has a radius of 5 cm. The dashed line position indicates the position where Eve's received power is equal to the leaked power. When the offset of Eve is 1.7 mm, 2.05 mm, and

3 mm respectively, its eavesdropping coefficient for OAM+5, OAM+3, and OAM+1 is 0. For a traditional Gaussian beam, Eve only needs to offset by less than 5 cm to intercept half of the beam's power. This indicates that the higher the order of the OAM modes the more difficult it is to eavesdrop. Figure S6(b) demonstrates the size of Eve versus the eavesdropping coefficient for an offset of 1 mm. When Eve's radius is 9.8 mm, 8 mm, and 5.4 mm, respectively, her eavesdropping coefficient for the OAM+5, OAM+3, and OAM+1 modes is zero. In the context of a traditional Gaussian beam, when Eve attempts to eavesdrop on half of the beam's power, the Eve 's radius is 3.5 mm. It's evident that eavesdropping on higher-order OAM beam requires a larger eavesdropper size.

Based on the above research, we can conclude that compared to communication systems based on Gaussian modes, Eve's eavesdropping on the OAM-CCL system for high-quality interception requires a larger size and positioning closer to the optical axis. But Eve's interception of the beam at such a close position will cause Bob's alarm. Even with the utilization of the most advanced optical beam splitter available, Eve would find it challenging to evade detection.[57] Consequently, we can infer that the OAM-CCL optical communication system has a high spatial resistance to eavesdropping.

6 System capacity and degree of freedom

For the OAM-CCL based communication system, the limit value of communication rate C_{lim} is obtained from the following equation:

$$C_{lim} = C_{max} \times (DoF - 1). \tag{S9}$$

Where C_{max} is the maximum communication rate in a single mode, its value is related to the bandwidth of the chaotic carrier and coefficient coefficient. Figure S7 shows the transmission rate versus BER for systems with different masking coefficients at OSNR = 20 dB. The single-mode transmission rates of the system with BER of HD-FEC are 12 Gb/s, 13 Gb/s, and 13.6 Gb/s when the masking factor is 0.35, 0.4, and 0.45, respectively. However, we generally do not choose such an extreme value. This is to ensure that the system is sufficiently robust to environmental changes.

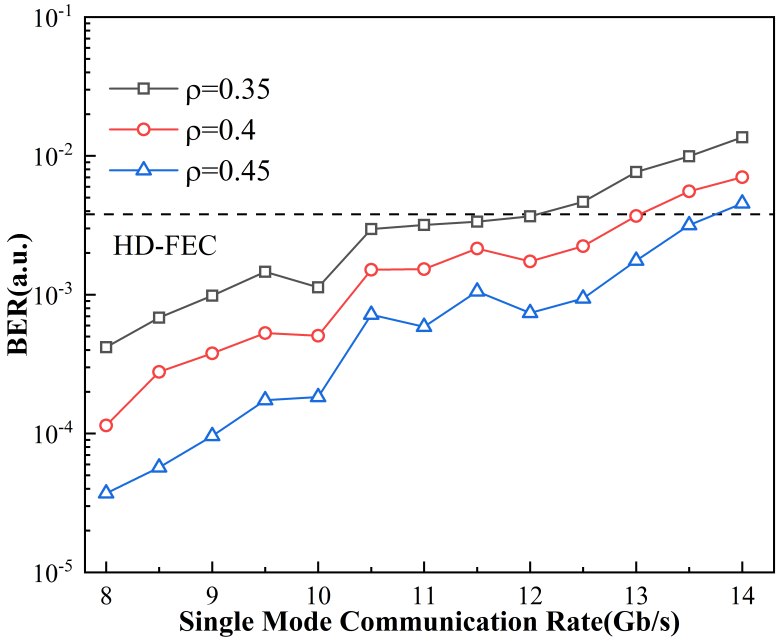

Fig S7 BER versus single-mode information rate for different masking coefficients.

The degree of freedom determines the multiplication of the capacity that the orbital angular momentum enhance and determines the potential of the system communication capacity. On the basis of Eq.1, letting $K = 2p + |l| + 1$, we can obtain the solution for the degrees of freedom of the OAM-CCL communication system:

$$DoF = \sum_{p=0}^{P_{max}} 2l_{max} + 1 = \lfloor \frac{K_{max}^2 + 1}{2} \rfloor , \tag{S10}$$

$$K_{max} = \max\{\frac{R_T^2}{\omega_0^2}, \frac{(2\pi R_R w_0)^2}{4\lambda^2(z^2 + z_R^2)}\}. \tag{S11}$$

Where $\lfloor \cdot \rfloor$ is rounding down, R_T is transmitter size, R_R is receiver size, z_R is Rayleigh distance, λ is wavelength. Figure S8 depicts the correlation between receiver size and degrees of freedom for various transmission distances. In the illustration, both the transmitter and receiver dimensions are fixed at 10 cm. As the receiver size expands, the system's degrees of freedom increase until they reach a peak value at 313. Beyond this point, the degrees of freedom no longer increase. Additionally, it is observed that for identical receiver sizes, larger transmission distances correspond to reduced degrees of freedom. This phenomenon arises from the increasing divergence of the OAM beam with distance, resulting in systems with closer distances exhibiting greater degrees of freedom for the same receiver size. Furthermore, once the receiver size surpasses a certain threshold, the transmitter size becomes a limiting factor for the system's degrees of freedom.

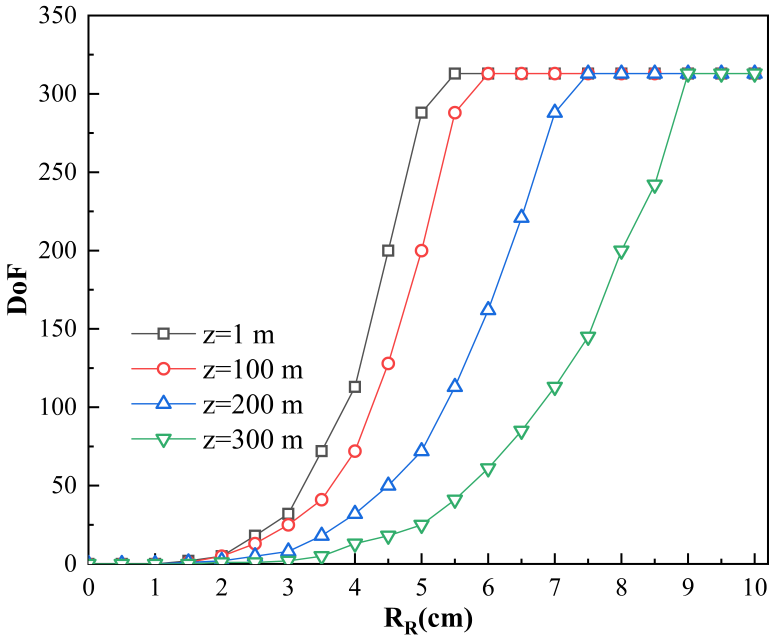

Fig S8 Receiver size versus system degrees of freedom.

7 System communication distance

The transmission distance of the system is mainly dependent on the size of the laser beam waist radius, which determines how much OAM light is dispersed, and the size of the receiver, which determines how efficiently the receiver receives power.Therefore, we can derive the formula for calculating the transmission distance of the system:

$$z_{\max} = \frac{\pi w_0^2}{\lambda} \sqrt{\frac{R_R^2}{w_0^2 \left(l_{\max} + 1\right)} - 1}\,. \tag{S12}$$

Where, l_{max} is the maximum topological load of the OAM mode, in our system the value is 11. z_{max} is the maximum transmission distance of the reference, once the transmission distance of the system exceeds this value, the BER of the system will become drastically worse. From this we can get the relationship between the transmission distance and the receiver size as well as the radius of the initial beam waist of the laser as shown Fig. S9.

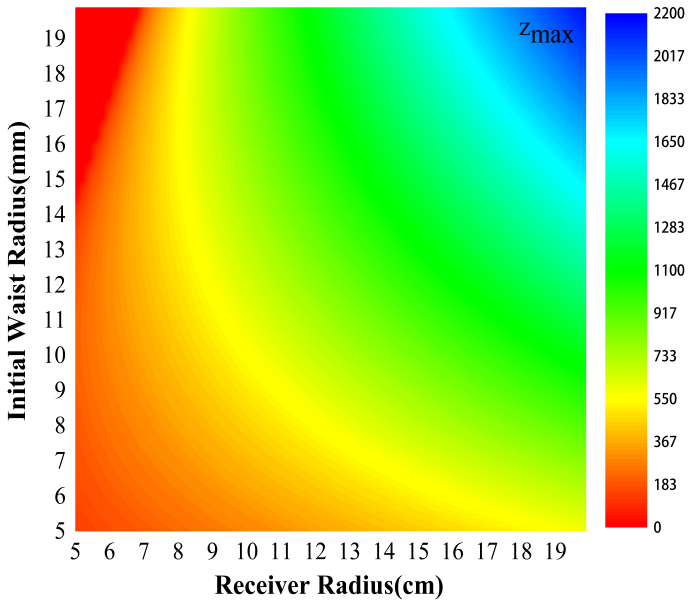

Fig S9 BER versus the message rate with different masking coefficients.

8 Transmitter and receiver misalignment

Figure S10 illustrates three typical scenarios of misalignment in the system. We numerically analyze the impact of three typical misalignment phenomena on the commonly-driven chaotic secure communication system.

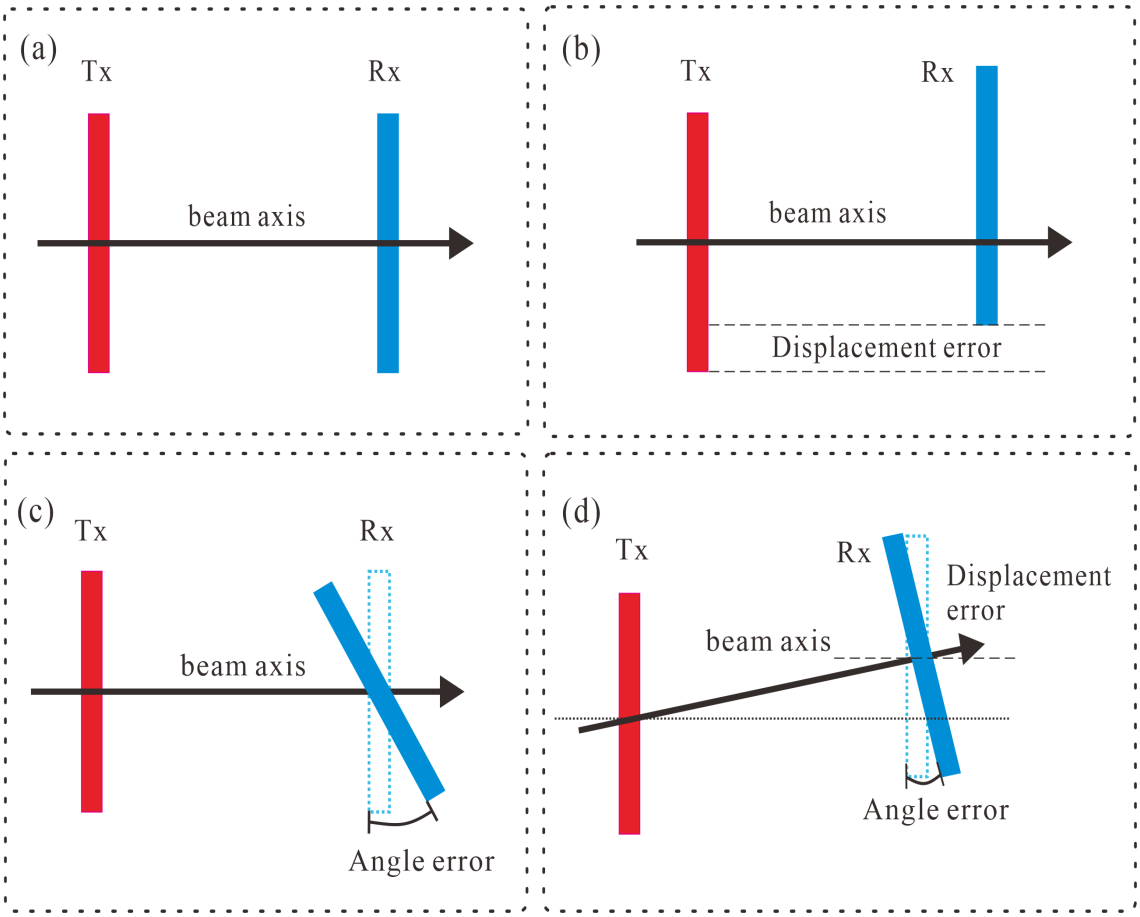

Fig S10 Concept of misalignment. (a) Perfect alignment of transmitter and receiver; (b) Displacement error between transmitter and receiver; (c) Angular error between transmitter and receiver; (d) Transmitter and receiver misalignment with both angular and displacement errors.

9 Displacement error between transmitter and receiver

It should be noted that in this section the transmission distance z is fixed to 1m in order to explore the effect of other parameters on the system. Figure S11(a) shows the variation of the orbital

angular momentum (OAM) spectrum of OAM + 1 mode resulting from the displacement error when ω_0 = 2 cm. It can be observed that as the lateral displacement increases, the power of the OAM + 1 mode continuously decreases, and there is continuous leakage to other modes. Moreover, it can be observed that the OAM + 2 and OAM + 0 modes experience higher crosstalk compared to the OAM - 1 and OAM + 3 modes. Figure S11(b) shows the power variation with increasing displacement error for OAM beams with different initial beam waist and topological charge. It can be seen that when a displacement error occurs, the smaller the initial beam waist, the greater the topological charge leading to more severe power degradation. In this paper, XT-n is defined as the relative power leaked by the OAM beam to a mode with a mode spacing of n. Figure S11(c) shows the variation of XT-1 for OAM + 1 mode with different initial beam waist and topological charges, indicating that larger initial beam waist and smaller topological charges lead to smaller XT-1 values, suggesting higher tolerance to displacement error. Similarly, In Fig. S11(d), the variations of XT-2 for OAM + 1 mode with different initial beam waist and topological charges are presented, showing a consistent trend with Fig. S11(c) but with smaller values compared to XT-1.

The fundamental consideration in system design for chaotic secure optical communication is to ensure a robust chaos synchronization performance, as it plays a pivotal role in the secure optical communication. From Fig. S11, it can be observed that higher OAM modes experience greater power loss when a displacement error occurs. Therefore, it is advisable to allocate the driving chaotic signal to smaller OAM modes to ensure sufficient robustness of chaotic synchronization against displacement error. Based on this conclusion, the driving chaotic signal is allocated to the OAM + 1 mode, while the encrypted signal is assigned to other modes. The BER and synchronization coefficient of the system are tested under different mode spacing when a displacement error occurs, as shown in Fig. S12.

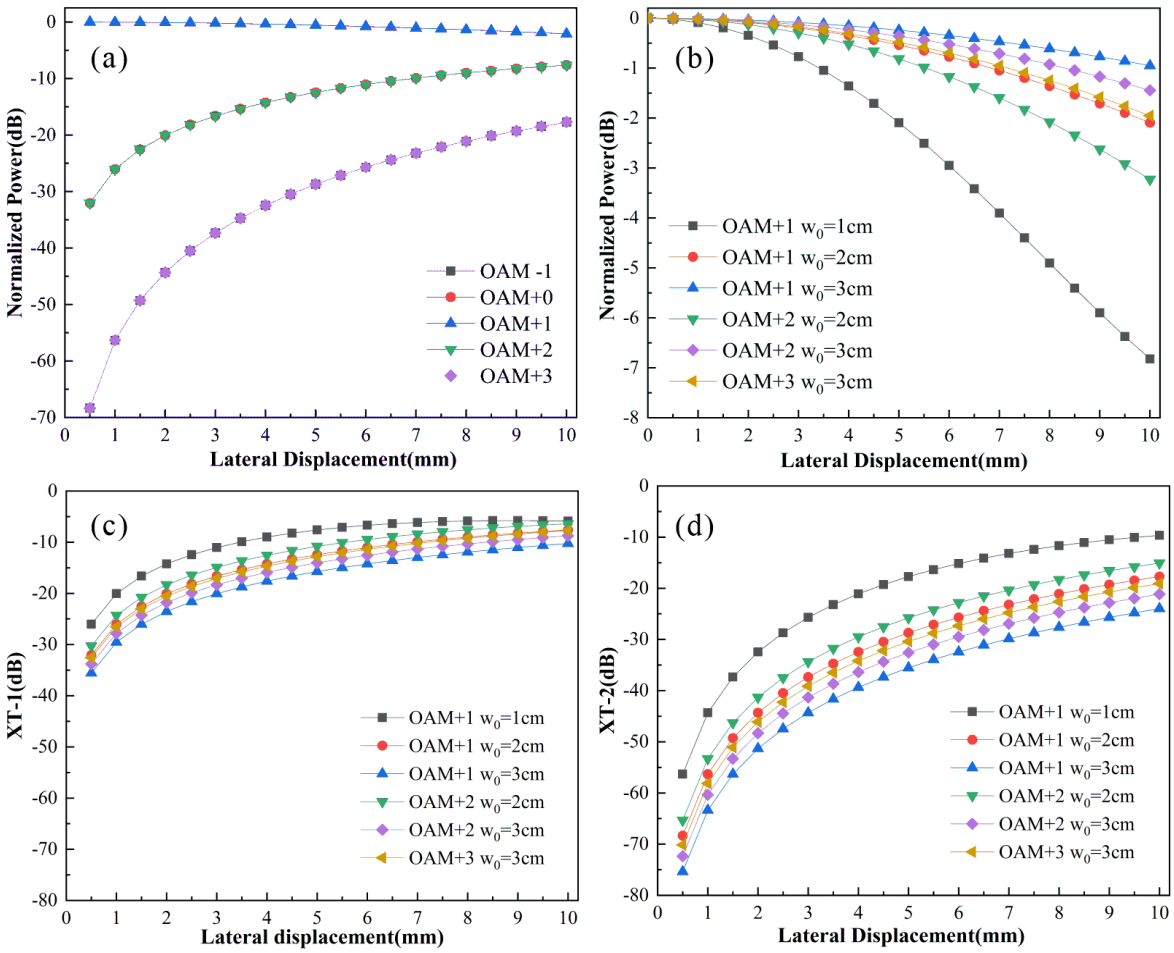

Fig S11 Power distribution under displacement error. (a) Power distribution when displacement error occurs with the transmitting mode as OAM + 1 and ω_0 = 2 cm; (b) Power attenuation when displacement error occurs with different OAM modes and different initial beam waist; (c) XT-1 as the function of lateral displacement with different OAM modes and different initial beam waist; (d) XT-2 as the function of lateral displacement with different OAM modes and different initial beam waist.

Figure S12(a) presents the crosstalk matrix between OAM modes when the displacement error is 2 mm and w_0 = 2 cm. Figure S12(b) illustrates the BER of the system as a function of lateral displacement under different mode spacings, with a masking coefficient of 0.187. The systems with mode spacings of 1, 2, and 3 reach the hard decision forward error correction (HD-FEC) threshold at lateral displacements of 1.4 mm, 3.9 mm, and 2.8 mm, respectively. Figure S12(c) shows the variation of the chaotic synchronization coefficient during this process. We can find that the communication quality of the system with mode spacing of 2 is significantly better than that of the

system with mode spacing of 1, but the communication quality of the system with mode spacing of 3 is worse than that of the system with mode spacing of 2. The main reason for this phenomenon is that while the mode spacing reduces the crosstalk between different modes, a larger mode spacing results in higher power loss in the system, leading to a degradation of the chaotic synchronization quality. It should be noted that the proportion of power loss and crosstalk to communication quality varies with the masking coefficient. Figure S12(d) shows the BER of the system as a function of masking coefficients under different mode spacing, with a displacement error is 2 mm. It can be observed that increasing the masking coefficient can improve the communication quality caused by displacement error, but it reduces the system's confidentiality performance. Therefore, the choice of the masking coefficient should be carefully considered in system design.

From the above results, it can be seen that chaotic secure communication is much more complex compared to general mode-division-multiplexing communication. The factors that affect the communication quality of the commonly-driven chaotic secure communication system when the displacement error occurs are: (1) The degradation of the chaotic synchronization coefficient due to the power loss of the driving chaos; (2) The degradation of the chaotic synchronization coefficient due to the degradation of the optical signal-to-noise ratio of the driving chaos; (3) The degradation of the signal-to-noise ratio of the encrypted signal; (4) The additional signal-to-noise ratio degradation caused by the mismatch between the encrypted signal and the synchronous chaotic power during the removal of chaotic masking signal. Since $\mathrm{SL_R}$ is an active laser, the power drop of the synchronous chaotic signal is much smaller than the power decay of the encrypted signal, leading to a power mismatch between the two and resulting in additional noise during the removal of chaotic masking signal.

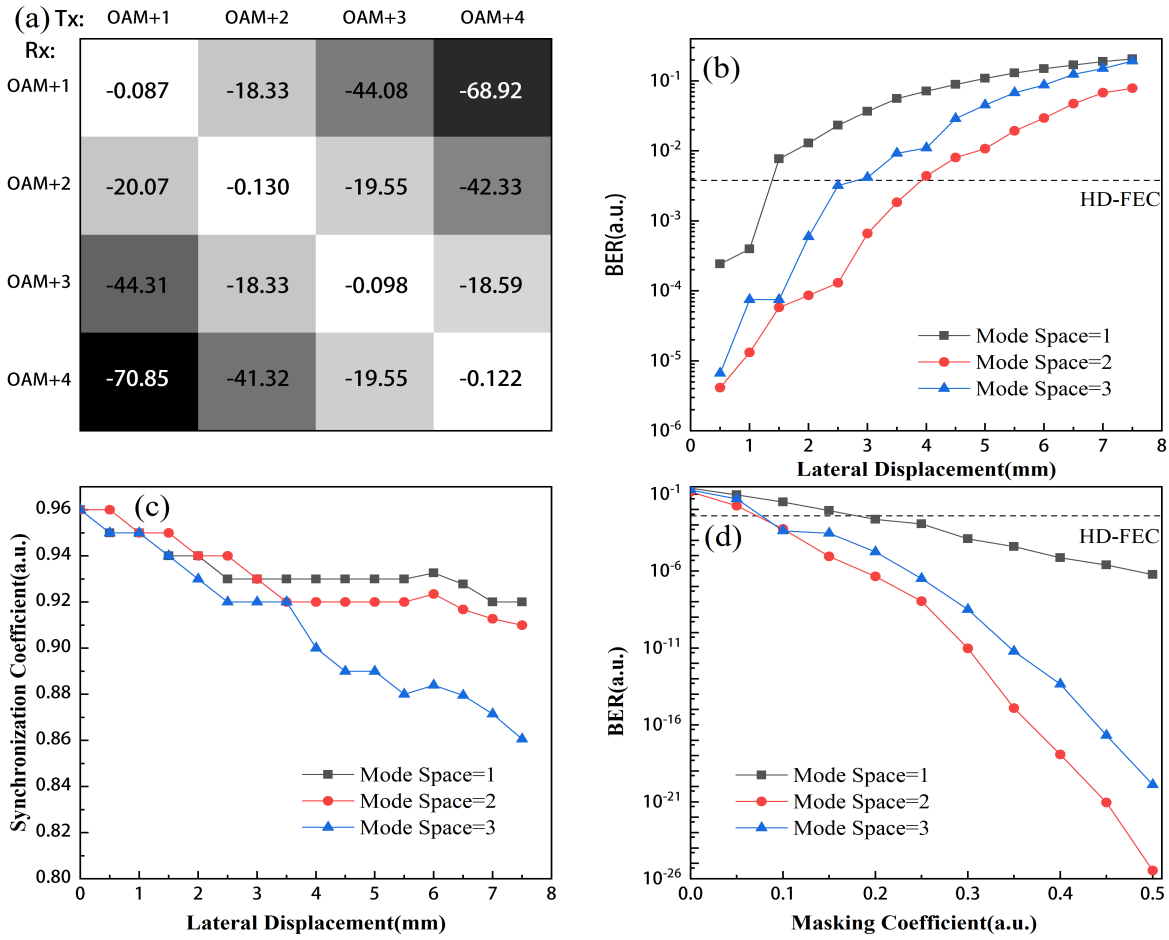

Fig S12 Communication performance under displacement error. (a) Crosstalk matrix between modes for a displacement error of 2 mm and w_0 = 2 cm; (b) BER variation with different mode spacing under displacement error, masking coefficient is 0.187; (c) Synchronization coefficient variation with different mode spacing under displacement error; (d) BER variation with different mode spacing and masking coefficients under a displacement error of 2 mm.

10 Angular error between transmitter and receiver

Figure S13(a) shows the change in OAM power distribution due to angular error when sending OAM + 1 with an initial beam waist of 2 cm. A larger angular error leads to stronger power attenuation and inter-mode crosstalk. Figure S13(b) shows the power variation with increasing displacement error for OAM beams with different topological charges and different initial beam waist. It can be observed that the larger the initial beam waist is, the more severe the mode attenuation is, which is different from the effect of the displacement error. Figure S13(c) and S13(d)

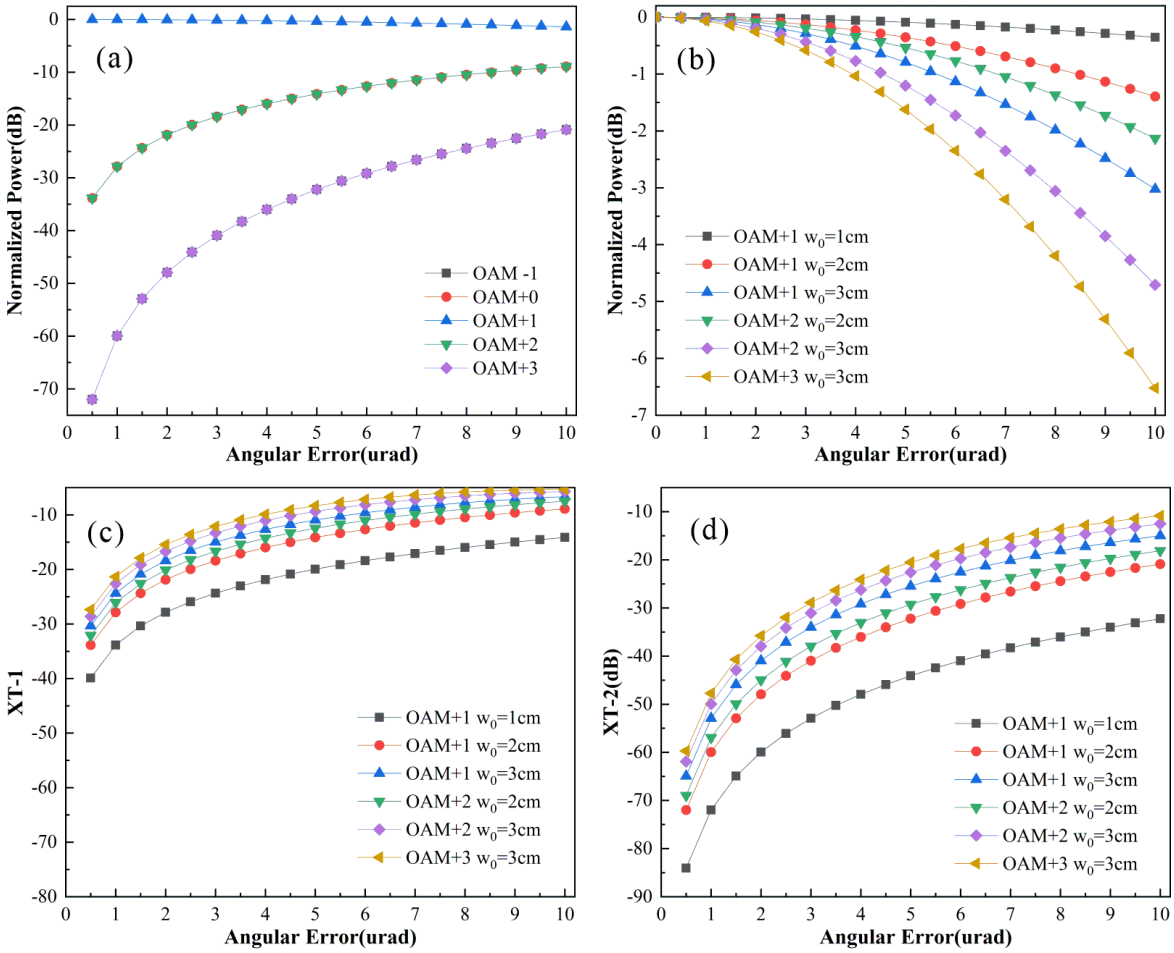

Fig S13 Power distribution under angular error. (a) Power distribution when angular error occurs with the transmitting mode as OAM + 1 and w_0 = 2 cm; (b)Power attenuation when angular error occurs with different OAM modes and different initial beam waist; (c) XT-1 as the function of angular error with different OAM modes and different initial beam waist; (d) XT-2 as the function of angular error with different OAM modes and different initial beam waist.

shows the variation of XT-1 and XT-2 for OAM beams with different initial beam waist and different topological charges. It can be observed that the larger the initial beam waist the smaller the XT-1 and XT-2, and the smaller the topological charge the smaller the XT-1 and XT-2, indicating that the mode with smaller initial beam waist is more tolerant to displacement error, which is the opposite of the situation at displacement error.

Similar to the displacement error analysis, the effect of angular error on chaotic synchronization and BER of the system is discussed in this section. Figure S14(a) shows the crosstalk matrix

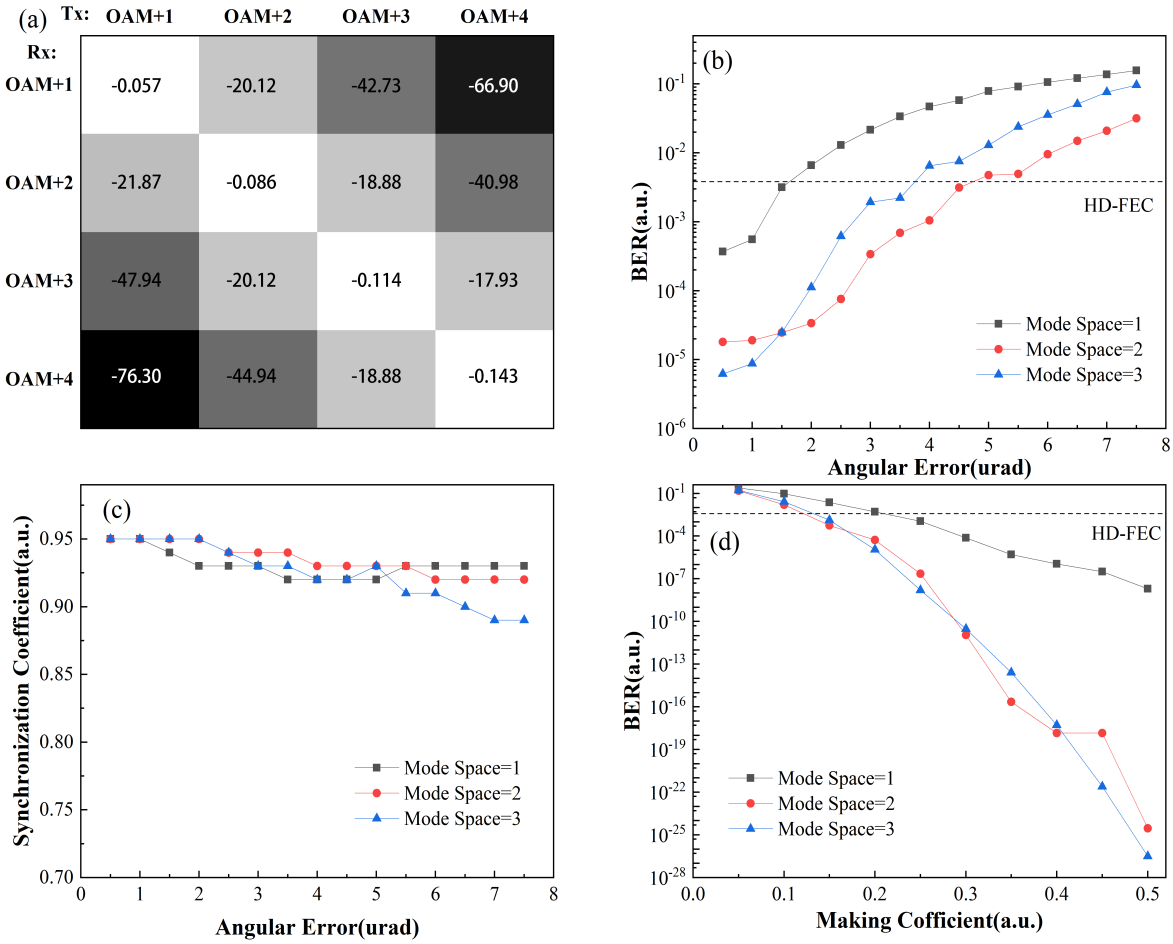

Fig S14 Communication performance under angular error. (a) Crosstalk matrix between modes for a angualr error of 2 mm and w_0 = 2 cm; (b) BER variation with different mode spacing under anguar error, masking coefficient is 0.187; (c) Synchronization coefficient variation with different mode spacing under angular error; (d) BER variation with different mode spacing and masking coefficients under a angular error of 2 mm.

among the modes of the OAM when the lateral displacement is 2 mm, ω_0 = 2 cm. Figure S14(b) shows the BER of the system as a function of the angular error with different mode spacing, when the masking coefficient is 0.187. The systems with mode spacing of 1, 2, and 3 reach the hard decision forward error correction (HD-FEC) threshold at angular error of 1.6 urad, 4.7 urad, and 3.7 urad, respectively. Figure S14(c) shows the variation of the synchronization coefficient in this process. Similar to the displacement error, although the larger mode spacing reduces the mode crosstalk, the system power loss makes the synchronization coefficient decrease, which in

turn makes the communication quality degrade. Figure S14(d) shows the variation of BER for systems with different mode spacing with different masking coefficient when the angular error is 2 urad. It can be seen that the performance of mode spacing 3 and 2 changes with different masking coefficient, which indicates that different masking coefficient affect the choice of mode spacing.

11 Simulation experiments

We set the size of both the transmitter and receiver to 20 cm, the initial beam waist of the LG beam to 2 cm, the OSNR to 20 dB, the transmission distance to 10 m. And we do not use any error correction mechanism in order to visualise the results.

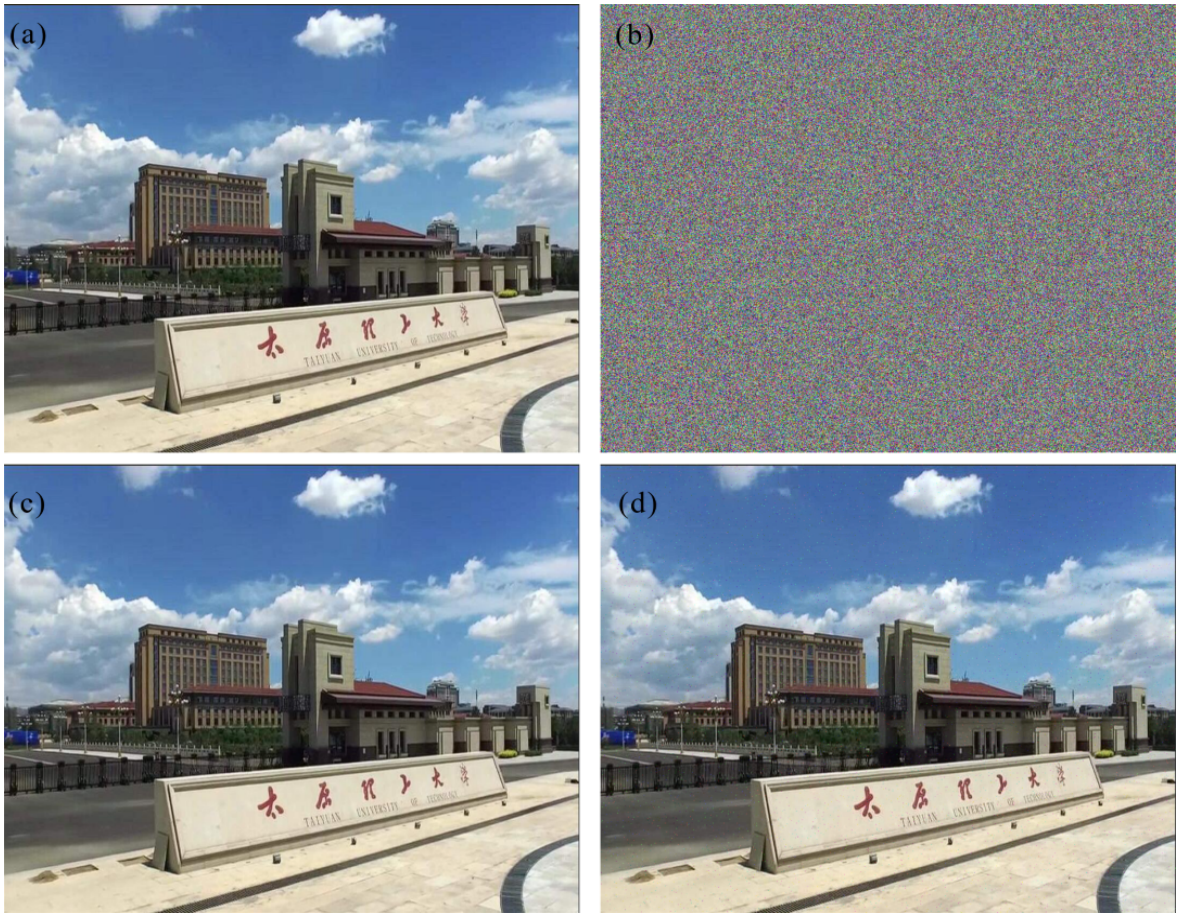

Fig S15 Simulation experiment of picture transmission in indoor environment. (a) Original image; (b) Encrypted images tapped by eavesdroppers; (c) Transmission distance of 10 m; (d) Displacement error is 1mm, angular error is 1 urad.

We modeled the images received by the eavesdropper, the legitimate receiver, and the misaligned receiver, respectively. We use peak signal-to-noise ratio (PSNR) and structual similarity (SSIM) to evaluate image quality.[55] The results show that it is difficult for eavesdroppers to break the encrypted message and our designed system is robust to misalignment, the details are shown in Fig. S15. Figure S15(a) shows the original picture. Figure S15(b) shows an encrypted image being eavesdropped on by an eavesdropper with a displacement error of 5 mm and an angular error of 5 urad.The image has a PSNR of 10.19 dB and a SSIM of 0.05. This implies that the encrypted image is severely distorted and has a very high variance from the original image. Figure S15(c) shows the encrypted image after it has been legally decrypted by the receiver. At this point, the PSNR of the image is 47.78 dB, and the SSIM is 0.99. This indicates that there is little or no degradation in the quality of the image. Figure S15(d) shows the decrypted image at a displacement error of 1mm and an angular error of 1 urad.The PSNR of the image is 31.34 dB and the SSIM is 0.95, which means that the image quality produces a degradation.

In addition, we simulate the communication performance of the OAM-CCL system in an environment of atmospheric turbulence by using the Kolmogorov theoretical model, as shown in Fig. S16. C_n^2 denotes the strength of atmospheric turbulence, $C_n^2 > 2.5 \times 10^{-13}\ m^{-2/3}$ means strong turbulence, $2.5 \times 10^{-13}\ m^{-2/3} > C_n^2 > 6.4 \times 10^{-17}\ m^{-2/3}$ means moderate turbulence and $C_n^2 < 6.4 \times 10^{-17}\ m^{-2/3}$ means weak turbulence. Figure S16 demonstrates the variation in the transmission quality of the pictures for different turbulence intensities and transmission distances. The PSNR for the four images were 40.19 dB, 39.97 dB, 33.46 dB, and 24.34 dB, and the SSIM was 0.99, 0.99, 0.95, and 0.77, respectively. Thus, it can be seen that under moderate turbulent transmission conditions, the system can still maintain a high quality of communication.

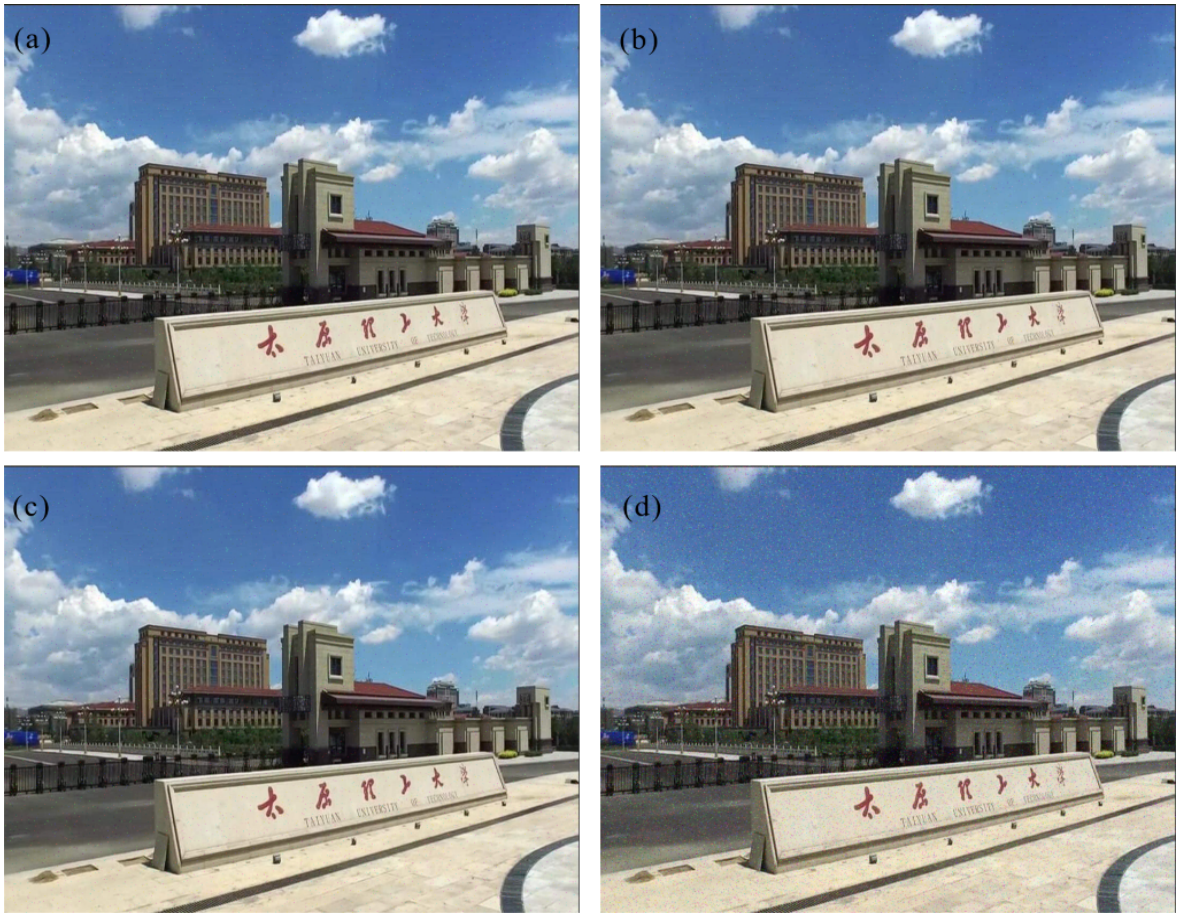

Fig S16 Simulation experiment of picture transmission in atmospheric turbulence environment. (a) $C_n^2 = 1 \times 10^{-16}\ m^{-2/3}$, $z = 1000\ m$; (b) $C_n^2 = 1 \times 10^{-16}\ m^{-2/3}$, $z = 2000\ m$; (c) $C_n^2 = 1 \times 10^{-15}\ m^{-2/3}$, $z = 1000\ m$; (d) $C_n^2 = 1 \times 10^{-15}\ m^{-2/3}$, $z = 2000\ m$.

12 Mode decomposition

For any beam in space can be considered as a superposition of different OAM beams:[43]

$$u(r, \phi, z) = \frac{1}{\sqrt{2\pi}} \sum_{m=-\infty}^{\infty} a_m(r, z) exp(im\phi)\,, \tag{S13}$$

where, $a_m(r, z) = \frac{1}{\sqrt{2\pi}} \int_0^{2\pi} u(r, \phi, z) exp(-im\phi) d\phi$. So, the energy weight of each OAM mode can be calculated as:[43]

$$C_m(r, z) = \int_0^R |a_m(r, z)|^2 r dr\,. \tag{S14}$$

For more information on how to decompose the misaligned OAM beam, the work of Vasnetsov et al. can be consulted.[46]

The near-axis limit of the beam described by the paraxial estimator is defined as follows:[42]

$$\mathcal{P} = \frac{\int_{-\infty}^{+\infty} Im\{E_p^* \partial_z E_p\} dxdy}{\int_{-\infty}^{+\infty} E_p E_p^* k dxdy}. \tag{S15}$$

So, the paraxial estimator of the LG beam was calculated as:[42]

$$\mathcal{P} = 1 - \frac{2p + |l| + 1}{(k\omega_0)^2}, \tag{S16}$$

where, k is the wave vector. The radius of the OAM beam $\sigma_r(z)$ can be calculated as:[41]

$$\sigma_r^2(z) = \frac{2\int_0^{2\pi}\int_0^{\infty} r^2 I(r,\phi,z) r dr d\phi}{\int_0^{2\pi}\int_0^{\infty} I(r,\phi,z) r dr d\phi}, \tag{S17}$$

where, $I(r,\phi,z)$ is the beam intensity. The radius of the LG beam $\sigma_r(z)_{lp}$ can be approximated as:[56]

$$\sigma_r(z)_{lp} = \omega(z)\sqrt{2p + |l| + 1}. \tag{S18}$$